Gas Separation in the Ranque-Hilsch Vortex Tube. Model Calculations Based on flow Data

Linderstrøm-Lang, C.U.

Publication date:
1966

Document Version
Publisher's PDF, also known as Version of record

Risö Report No. 135

Risö Report No. 135

Danish Atomic Energy Commission

Research Establishment Risö

Gas Separation in the Ranque-Hilsch Vortex Tube
Model Calculations Based on Flow Data

by C. U. Linderstrøm-Lang

June, 1966

Sales distributors: Jul. Gjellerup, 87, Sölvgade, Copenhagen K, Denmark

Available on exchange from: Library, Danish Atomic Energy Commission, Risö, Roskilde, Denmark

June, 1966 Risö Report No. 135

Gas Separation in the Ranque-Hilsch Vortex Tube. Model Calculations Based on Flow Data

by

C. U. Linderstrøm-Lang

The Danish Atomic Energy Commission
Research Establishment Risö
Chemistry Department

Abstract

In a previous publication[1] a number of experimental data were presented, showing the gas-separation ability of a series of Ranque-Hilsch vortex tubes. It was concluded that the driving force behind the observed effects is the centrifugal field. In the present paper this result is used for the calculation of the separation potential of the tubes from estimated tangential-velocity distributions[2]. A simple model of the secondary flows in the tubes is shown to provide a basis for a quite accurate reproduction of most of the gas-separation results obtained previously.

Contents

1. Introduction

Gas separation in a series of vortex tubes has been studied previously[1]. Rather complex results were obtained, which, however, showed regularities that permitted a fairly satisfactory qualitative interpretation. In the following an attempt will be made to reproduce both qualitatively and quantitatively the gas-separation results obtained in ref. 1 from estimated tangential-velocity distributions determined in ref. 2 on the basis of wall-pressure measurements.

2. Nomenclature

"cold" : End of tube adjacent to jet.

"hot" : End of tube away from jet.

D : Diameter of tube.

d_c and d_h : Diameters of cold and hot orifice respectively.

$r_c = \frac{1}{2} d_c$; $r_h = \frac{1}{2} d_h$; $r_p = \frac{1}{2} D$.

r_f : Radius of maximum tangential velocity, v_f.

r^* : Radius of inner cylinder with reversed flow (fig. 5).

z_o : Length of tube.

z_c and z_h : Lengths of the two separating surfaces (fig. 3).

v_j : Inlet velocity.

b : Velocity reduction at jet.

v : Tangential velocity.

v_p : bv_j.

n : Exponent in assumed power law for v, $v \infty r^n$. For $r < r_f$, $n = 1$; for $r > r_f$, $-1 < n < +1$.

m : Exponent in assumed power law for the radial distribution of axial flow; $m = \log(\theta_o/(1-\theta_o))/\log(d_h/d_c)$.

N : Concentration in mole fraction of the lighter component.

N_o : Concentration of inlet flow.

N'_o : Average concentration of flow in body of tube.

N_{wc} and N_{wh} : Concentrations of flow in end-wall boundary layers.

N_c and N_h : Concentrations of cold and hot stream respectively.

dN : $N_c - N_h$.

N'_c and N'_h : Concentrations of cold and hot exit stream, excluding direct flow from boundary layers.

L : Inlet-flow volume in moles per time unit.

L_{wc} and L_{wh} : Flow volumes in end-wall boundary layers directly to exit (fig. 3).

L' : Flow volume in body of tube, $L' = L - L_{wc} - L_{wh}$.

$L^{\varkappa}$: Flow volume in inner cylinder with reversed flow (fig. 5).

θ : Flow fraction through hot exit (fig. 3).

θ' : $(\theta L - L_{wh})/L'$.

$(1-\theta')$: $((1-\theta)L - L_{wc})/L'$.

θ_o and θ'_o : θ and θ' with open valves at both ends.

$\theta^{\varkappa}$: $= \dfrac{L_c^{\varkappa}}{L'_h + L_c^{\varkappa}}$ for $\theta < \theta_o$; $= \dfrac{L_h^{\varkappa}}{L'_c + L_h^{\varkappa}}$ for $\theta > \theta_o$ (fig. 5).

u_c etc. : Rates of diffusional separation or separative exchange in radial direction per cm tube length (fig. 3):

$$u = 2\pi \frac{D_f p}{RT} \frac{\Delta M}{RT} v^2 N(1-N) .$$

D_f : Coefficient of diffusion

ΔM : Molecular weight difference.

R : Gas constant.

T : Absolute temperature.

3. The Secondary-Flow Pattern

It was concluded in ref. 1 that, in spite of the complexity of the results, the vortex tube acts essentially as a centrifuge, i. e. that pressure diffusion is responsible for at least the major part of the separation. The results were explained on the basis that axial flows play an important role in establishing the net gas-separation effect, i. e. the effect measured at

the outlets, and that the main region of separation is within a rather narrow cylinder about as wide as the larger of the two orifices.

In ref. 1, fig. 11, it was postulated that the separating region constituted a so-called con-current column, in the case concerned in principle two adjacent annular regions with axial flow in the same direction and separated by a cylindrical surface through which the separative exchange took place. Here, on the other hand, it will be assumed that the separating region is in principle a counter-current column, i.e. it consists of two adjacent annular regions with separative exchange across the boundary, but here with the flows in opposite directions (see fig. 1). The maximum possible gas separation is not much different in the two cases, but the counter-current concept is used here because it appears to be more in line with flow visualization experiments (see below) and, equally important, because it has been impossible to develop a satisfactory flow model on the basis of the con-current concept.

It is assumed that back diffusion plays but a minor role. This is possible, as indicated by Cohen[3], because the flow volume per second through the tube is very large. Therefore the separative diffusion at any point in the tube is a function of the centrifugal field only, an assumption which considerably simplifies the mathematical treatment and makes it easy to identify the regions of the tube that contribute to any extent to the net gas-separation effect measured between the two outlets.

The numerical results obtained in this way are in agreement, as regards order of magnitude, with the theoretical maximum separation obtainable from the tube, as measured in terms of separative work[3] and with due regard to the turbulence in the tube[4].

According to fig. 1, the secondary flows in the tube, especially the axial, play an important role in the creation of the separation effect. During the last few years a number of features of this flow pattern have been investigated, in particular the redistribution flow at intermediate radii. There is now sample evidence, especially from flow visualization experiments[5-9] that such flows are easily established, if not always present. Theoretical calculations[7, 10-12] have shown that they are caused by the ejection of mass flow from the end-wall boundary layers; however, only the completely symmetrical situation has been considered. This is unfortunate since in that case no net gas-separation effect of the type discussed here can arise. Extension of the theory to cover the present case would meet with considerable difficulty since any flow pattern encountered in practice is determined by the balancing of a number of factors that are undoubtedly very sensitive to

changes in the end-wall boundary layers. A quantitative treatment from first principles is therefore out of the question at present. This being so, it might be worth while instead to find the most probable flow patterns compatible with the experimental separation results referred to above. This approach might provide useful insight into the working mechanism of the vortex tube. In fact this seems to be possible, mainly because a long series of experimental results with varied parameters[1] has shown regularities that leave very little room for variation in the interpretation of the separation data, not to mention the fact that the appearance of a net separation effect of a particular sign in itself restricts the number of possible flow patterns considerably, as indicated above.

As a basic requirement and in agreement with theory and flow visualization experiments, it is assumed that ejection from the end walls takes place near or at the exit radius, giving rise to annular layers of axial flow with a high degree of mixing within the layers, but less between them.

It follows that the basic secondary-flow pattern in the vortex tubes under investigation may be depicted as shown in fig. 2, which also indicates the type of vortex tube employed here (the ratio of the flows through the two exits can be changed to any value by means of two valves downstream of the exit ducts). The mass flow in the boundary layers is divided at the orifice, one fraction passing directly into the exit duct.

The most important change in the results of refs. 8 and 9 to fit the present situation with two exits is that the stagnation point at the centre may have any position along the axis; in fact this is a major point in the hypothesis developed below.

The examples from fig. 2 are shown again in fig. 3 with separating surfaces (fig. 1) included.

According to the simplified picture described above, no other region in the main body of the tube can contribute to the separation. Experiments with exits at the periphery (see ref. 1) have, however, shown that the flow volume carried along the peripheral wall has undergone a small change in concentration, probably on entering the tube through the nozzle.

4. Separation at $\theta = \theta_c$

It is quite easy to show from mass-balance considerations that, with the notations of fig. 3, the net concentration changes in the two exit streams are

$$N_c - N_o = \frac{1}{(1-\theta)L}\left(\theta' u_c z_c - (1-\theta')\, u_h z_h + \theta' L_{wc}(N_{wc} - N_o) - (1-\theta')L_{wh}(N_{wh} - N_o)\right) \quad (1)$$

and

$$N_h - N_o = -(N_c - N_o)\,\frac{(1-\theta)}{\theta} \quad , \quad (2)$$

where the L's are moles of flow per time unit and the N's are mole fractions of the lighter component; u_h and u_c are the net transfers of the lighter component inward per cm tube length.

The net transfer, u, is proportional to the centripetal acceleration and to the radius at which the gas separation takes place, i. e. u is proportional to the square of the tangential velocity. Thus the first two terms in the expression have opposite signs, and the two separating regions z_c and z_h actually compete with each other. On top of this there is a small contribution to the gas-separation effect from that part of the end-wall flows which passes directly into the exit ducts; $N_{wh} - N_o$ can be estimated from the experiments in ref. 1 referred to above.

The ratio of the two net transfers, u_c/u_h, depends on the relative widths of the two orifices, but since the tangential velocity has a maximum at a relatively small radius, this relationship is not simple.

Fig. 3 refers to the situation with unrestricted flow through the exit ducts, i. e. with the downstream valves open. From the above considerations it is clear that the sign and magnitude of the net separation effect actually measured depend on several parameters under these conditions. In agreement with this it is found experimentally that separation effects dN of both signs do in fact occur when both valves are open (see ref. 1, fig. 6; the broken line tentatively drawn in that figure may be taken to indicate that the stagnation point near the axis in fig. 3 of the present paper is closest to the narrower orifice, since, according to the flow picture in fig. 3, this will tend to produce a heavier flow fraction through the narrower than through the wider exit duct).

The sensitivity of the net gas-separation effect to changes in tube parameters was clearly brought out in some separation experiments in which the surfaces of the end walls of the vortex tube were made uneven by placing small lumps of glue near the exit radius (see fig. 4). In similar experiments by Ross[9] the effect of using a stepped end-wall surface has been investigated. He concluded that it leads to an increase in boundary-layer flow at the end wall in question, which flow is discharged at the step.

In the present experiments, conducted with tubes with orifices as shown in fig. 4, it was found that the sign of the net gas-separation effect is dependent on the end-wall surfaces in such a way that an uneven cold end wall (fig. 4a) produces a large positive effect, i. e. a heavier hot stream than cold, while an uneven hot end wall produces a fairly large negative effect, i. e. a heavier cold stream than hot. Furthermore, with both end walls smooth or uneven, the separation effects are in between. These results become intelligible if an increase in flow ejection near an exit radius is accompanied by changes in the flow pattern of the type shown schematically in fig. 4. It should be noted that the ratio of hot gas to cold did not change as a result of these modifications.

Similar experiments were conducted with a tube with large orifices, but in these cases the results were not so clear-cut, probably because the disturbance created by the uneven end walls had a profound effect on the tangential velocity also; at any rate the ratio of hot gas to cold was found to change appreciably.

The results obtained in ref. 1 (fig. 8) with tubes in which a thin-walled, coaxial tube was substituted for one of the orifices (as in a cyclone) undoubtedly have a similar explanation rather than that offered in ref. 1 since the tube will enhance the axial flow along the inner tube away from the end wall. As a matter of fact the curves in ref. 1, fig. 8, are very similar to the gas-separation curves obtained with uneven end walls (unpublished results).

5. Separation at $\theta \neq \theta_o$

If one of the valves downstream of the exit ducts is partly closed, a new situation arises. The resulting pressure increase in the exit duct will first affect the outflow along the centre axis because of the radial pressure gradient; in fact it may conceivably stop it altogether without reducing the outflow at the periphery appreciably.

This applies to tubes with fairly narrow orifices, as discussed in ref. 2. In tubes with wider orifices there is the possibility that the centre flow goes into instead of out of the tube.

With the centre flow through one exit stopped, the turning point of the flow in the corresponding cylinder may have moved to the exit or even further, according to the rate at which the rotation is dissipated in the duct. Experiments with a wire across an exit duct near the orifice (of 2 mm di-

ameter) gave little change in the gas-separation curve, indicating that the exit ducts do not play a vital part in its creation. The simplest pattern that may result under these conditions is indicated in fig. 5.

It is seen that, if this picture is correct, a new separating surface has been created. The flow model described below is based on this possibility. Its merit is, if nothing else, that with it a surprisingly close correlation between calculated and experimental separation effects is obtained.

Disregarding for a moment L_{wc} and L_{wh} of fig. 5, we may obtain the following expressions, using mass-balance considerations: 1. $\theta < \theta_o$, fig. 5b, where θ_o is the hot flow fraction obtained with open valves:

$$(1-\theta')L(N'_c - N'_o) = \theta' u_c z_c - (1-\theta')u_h z_h + \theta^{*} u_h z_h + (1-\theta^{*})u^{*} z_h \quad , \tag{3}$$

where $\theta^{*} = \dfrac{L_c^{*}}{L'_h + L_c^{*}}$, and

2. $\theta > \theta_o$, fig. 5a:

$$(1-\theta')L'(N'_c - N'_o) = \theta' u_c z_c - (1-\theta')u_h z_h - \theta^{*} u_c z_c - (1-\theta^{*})u^{*} z_c \quad , \tag{4}$$

where $\theta^{*} = L_h^{*}/(L'_c + L_h^{*})$.

At $\theta' = \theta'_o$ (i.e. $\theta = \theta_o$) $u^{*} = 0$; $\theta^{*} = 0$, and

$$(1-\theta'_o)L'(N'_c - N'_o) = \theta'_o u_c z_c - (1-\theta'_o)u_h z_h \quad , \text{ as before.} \tag{5}$$

The following crude approximations are now made: (1). With a decrease in flow volume through an exit tube caused by the closing of a valve, the outflow through that exit within a cylinder dependent on the degree of closing is stopped and reversed, while outside this region the outflows through the exits are not affected. The radius of the cylinder in question is identified with r^{*} of fig. 5. (2). The reversed flow is identified with L_c^{*} for $\theta' < \theta'_o$ and with L_h^{*} for $\theta' > \theta'_o$.

A rough estimate of r^{*} may be made in the following way:

Momentum considerations indicate that about equal volumes of flow are carried away within cylinders of equal radius through the two exit ducts when the pressures downstream, i. e. outside the tube, are equal. It follows

that in tubes with unequal exit-duct radii the flow ratio (hot to cold), in the case of unrestricted flows, is an indicator of the radial distribution of the flow volume through the wider duct. A simple power law being assumed to exist, namely $L_r \sim r^m$, where L_r is the flow volume carried within the cylinder r so that $m = \log(\theta_o/(1-\theta_o))/\log(r_h/r_c)$, m is found from experiments to be typically 3 to 4, a result that would appear very reasonable. It follows that $r^* \sim L^{*\,1/m}$.

A generalization of the above assumptions that permits L to be a function of θ, as is the case in tubes with narrow orifices, runs as follows: For $\theta' < \theta'_o$

$$\theta^* = (\theta'_o - \theta')/\theta'_o \quad \text{and}$$

$$r^* = r_h\left[(\theta_o - \theta)/\theta_o\right]^{1/m} .$$

In the second equation the overall mole fraction θ has been used instead of θ'; the distinction is not great. In a similar way we have for θ' θ'_o

$$\theta^* = (\theta' - \theta'_o)/(1 - \theta'_o) \quad \text{and}$$

$$r^* = r_c\left[(\theta - \theta_o)/(1 - \theta_o)\right]^{1/m} .$$

The above assumption leads to the difficulty that it is hardly realistic that L_h^* and L_c^* in figs. 5 a and b increase all the way up to $\theta' = 1$ or down to $\theta' = 0$, respectively. Since the values of m are typically fairly large, this problem will, however, be of minor importance, for u^* will quickly approach u_c (in eq. (4)) or u_h (in eq. (3) so that θ^* in the limit disappears from the equations.

It is seen that $N'_c - N'_o$ is positive at least near $\theta' = 0$ and negative at least near $\theta' = 1$. At $\theta' = 0$ and $\theta' = 1$

$$(1 - \theta')L'(N'_c - N'_o) = 0.$$

Introduction of the expressions for θ^* into eqs. 3 and 4 leads to

$$(\theta' < \theta'_o)\ \text{fig. 5b:}\quad (1-\theta')L'(N'_c-N'_o) = \theta'(u_c z_c + u_h z_h + \frac{1}{\theta'_o}(u^*-u_h)z_h) \qquad (6)$$

and

$$(\theta' > \theta'_o)\ \text{fig. 5a:}\quad (1-\theta')L'(N'_c-N'_o) = -(1-\theta')(u_c z_c + u_h z_h + \frac{1}{1-\theta'_o}(u^*-u_c)z_c) . \qquad (7)$$

Finally,

$$N_c - N_o = \frac{1}{(1-\theta)L}\left[(1-\theta')L'(N'_c - N'_o) + \theta' L_{wc}(N_{wc} - N_o) - (1-\theta')L_{wh}(N_{wh} - N_o)\right] \quad (8)$$

and

$$N_h - N_o = -\frac{1-\theta}{\theta}(N_c - N_o) . \quad (9)$$

6. Parameters

The majority of the parameters in these equations are deducible from experimental data. The most important of them, the transfer quantities, are found from the equation

$$u = 2\pi \frac{D_f p}{RT} \frac{\Delta M}{RT} v^2 N(1-N) .$$

Here D_f is the coefficient of diffusion, Δ M the difference in molecular weight between the two components, R the gas constant, T the absolute temperature, and v the tangential velocity. As discussed in ref. 2, the radial distribution of the tangential velocity v may be written as proportional to r^n where n, in the outer part of the vortex tube, is a constant between -1 and + 1 and, near the centre, a constant close to + 1 (a forced vortex), with a sharp transition between the two regions. The v to be used in a given case is found in the following way: The measured value of the total flow volume through the tube gives the jet velocity, the data from ref. 2, table 1, provide a reasonable value for the velocity reduction taking place at the jet, and from the same table n is found. Finally the radius r_f at which the n-transition takes place is calculated from a simple interpolation formula $r_f = 2/3((1 - \theta)r_c + \theta r_h)$, and with this information v at any radius may be calculated. Some variation in these parameters can, however, be permitted on account of the limited accuracy of the velocity determinations.

Little is known of L_{wc} and L_{wh}, the parts of the end-wall boundary flows that pass directly into the exit ducts. A strong proof of their existence is found in the results of ref. 1, fig. 9, which shows that normally there is very little correlation between the temperature effect and the gas separation effect; if otherwise the flow picture used above is correct, there is little other possibility of explaining this lack of correlation than to ascribe it to the effect of a considerable L_{wh} or L_{wc}.

The order of magnitude of $N_{wh} - N_o$ is known from the "4-exit" experiments described in ref. 1, fig. 7. The same experiments indicate that $N_{wc} - N_o$ may be of the same order of magnitude and, somewhat surprisingly, even of the same sign.

7. Discussion

A parameter study of the preceding equations is shown in figs. 6 to 10; figs. 6 to 8 are based solely on the experimental flow data described above - though a small wall flow is included in order to make the solutions finite. Fig. 9 shows the effect of changing the end-wall flows and their concentration relative to the main flow, and fig. 10 shows the effect of changing m, the parameter which according to the theory determines the radial distribution of the axial flow through the orifices; the figure also shows the effect of changing the position of the stagnation point along the axis. In figs. 11-13 the best fit to some experimental curves is sought, the parameter values being kept within limits compatible with the accuracy of the flow dynamics data.

Comparison of the figures with the results of ref. 1 immediately shows that the basic pattern of the curves is reproduced very well; for one thing there is a maximum value of separation at a relatively small hot flow fraction θ and a "minimum" value at a higher θ, where, as always, a positive effect means that the hot stream is heavier than the cold, while the opposite is indicated by a negative effect.

Furthermore fig. 6 shows that the dependence of the separation pattern on the ratio of the orifice diameters, d_h/d_c, is reproduced both with regard to the displacement of the point of inversion towards higher θ with increasing d_h/d_c and with regard to the ratio of the numerical values of the maximum and minimum, which is seen also to increase with increasing θ (cf. ref. 1, figs. 2 to 4 and 10), see also fig. 11.

These results may now be interpreted in terms of the model. With unrestricted flow through the orifices ($\theta = \theta_o$) there are two regions of the tube which give rise to gas-separation effects, but they oppose one another so that a medium net separation effect is produced. The increased pressure on the axis resulting from the partial closing of one or the other exit produces a new separating surface. This surface will move away from the axis as the hot flow fraction decreases or increases, that is to say, sooner or later it will dominate the picture so that finally the whole tube co-operates in pro-

ducing an effect of one or the other sign; thus the slope of the separation curve is negative on both sides of θ_o. The return to zero effect at low and high θ is caused by the admixture of wall flow, which gains in importance under these conditions.

The change in the relative magnitudes of the maximum and minimum with changing d_h/d_c reflects the fact that the addition of a relatively light flow fraction along the axis to one or the other exit stream will have the greatest effect on the smallest flow volume, i. e. (for $\theta_o > 1/2$) when $\theta < \theta_o$, while in addition the end-wall flow masks the development of the third separating surface when, for $\theta_o > 1/2$, θ approaches one.

Fig. 7 reproduces the result, referred to in ref. 1, that the width of the orifices as compared with the tube diameter has an effect on the numerical values of the maximum and minimum in that (1) these increase with decreasing orifice diameters until a certain point below which there may be some reduction, and (2) the maximum and minimum become steeper with decreasing orifice diameters. The results in ref. 2 have shown that the radius of maximum tangential velocity moves inward with decreasing orifices and that at the same time this velocity increases so that the rate of separative exchange also increases, leading to a better separation. On the other hand, with sufficiently narrow orifices the jet velocity drops below sonic (see ref. 2) and the peripheral velocity decreases correspondingly, so that a maximum in separation ability occurs at some medium-size orifice radii. The decrease in flow volume which accompanies the jet velocity reduction will, however, somewhat oppose the corresponding reduction in the concentration difference.

With narrow orifices the tangential velocity greatly decreases when one or the other valve is closed; this may explain why the maximum and minimum become steeper the narrower the orifices.

Fig. 8 reproduces the result referred to in ref. 1 (see e. g. fig. 5) that the tube length has a profound effect on the separation curve. The fact that the best separation is found in relatively short tubes is to be attributed to the change in the velocity profile shown in ref. 2 to take place with increasing tube length. The extreme cases are not very accurately determined, and, as seen from a comparison of fig. 8 with fig. 13, a somewhat smaller value for n, perhaps negative, is more likely in the longest tube. As discussed in ref. 2, the flow in this tube is highly three-dimensional, and the n-value selected for the curve in fig. 8 is only an average value which may have little importance for that region of the tube in which the dominating separation takes place.

Fig. 9 shows how the direct end-wall flows may modify the separation picture, modifications which are similar to the diversity of patterns found in the experimental separation curves (see ref. 1 and figs. 11 to 13).

Fig. 10 shows that, for a given d_h/d_c ratio, both m and z_c/z_h modify the shape of the separation curve. The way in which this happens is, however, only in qualitative agreement with experiment (see figs. 11-13): According to the theoretical flow picture a proper m may be selected and z_c/z_h adjusted so that a correct separation occurs at $\theta = \theta_o$. This is indeed possible to some extent, but, as seen in figs. 11-13, the correct ratio between the numerical values of the maximum and minimum cannot be reproduced; the ratio changes too rapidly with changing d_h/d_c as compared with experiment. This discrepancy may be connected with the fact that the model assumes perfect mixing within each annular layer, a condition that may not be fulfilled in thick layers. This failure constitutes the limitation of the model; in all other respects it is thought to reproduce the main features of the experimental separation patterns quite satisfactorily (see figs. 11-13).

It will be seen from figs. 11 to 13 that also the order of magnitude of the calculated separation effects is in agreement with the experimental values, while at the same time the adjusted parameters do not deviate more than reasonable from the parameter values determined in ref. 2. This result is further tested in fig. 14, where a number of experimental maximum and minimum values are compared with the corresponding calculated values. It is here assumed that the separation takes place at that cylinder surface at which the tangential velocity is at a maximum (i. e. at $v = v_f$) and that the whole of the tube length co-operates in producing the effect.

The results in fig. 14 are seen to differ by a factor of less than 3 from the experimental values. The low efficiency of the tube at large r_f/r_p (large orifices) may indicate that the axial flows in these cases are different from what has been assumed here.

Similar calculations have been carried out for a number of vortex tubes with 6 mm diameter on the basis of the flow data obtained with the 10 mm tubes in ref. 2, and it has been found that the calculated values are in general somewhat too small (a factor of two to six) as compared with the experimental ones. The same applies to the $13\frac{1}{2}$ cm long tubes.

Bibliography

1. C. U. Linderstrøm-Lang, Gas Separation in the Ranque-Hilsch Vortex Tube. Int. J. Heat Mass Transfer 7, 1195 (1964).

2. C. U. Linderstrøm-Lang, An Experimental Study of the Tangential Velocity Profile in the Ranque-Hilsch Vortex Tube. Risö Report No. 116 (1965).

3. K. Cohen, The Theory of Isotope Separation (McGraw-Hill, New York, 1951).

4. M. L. Rosenzweig, W. S. Lewellen and J. L. Kerrebrock, Feasibility of Turbulent Vortex Containment in the Gaseous Fission Rocket. J. Amer. Rocket Soc. 31, 873 (1961).

5. A. J. Reynolds, A Note on Vortex-Tube Flows. J. Fluid Mech. 14, 18 (1962).

6. J. M. Kendall, Experimental Study of a Compressible Viscous Vortex. Techn. Report No. 32-290, Jet Propulsion Laboratory, California Institute of Technology (1962).

7. M. L. Rosenzweig, W. S. Lewellen and D. H. Ross, Confined Vortex Flows with Boundary-Layer Interaction. Report No. ATN-64 (9227)-2 (1964).

8. M. L. Rosenzweig, D. H. Ross and W. S. Lewellen, On Secondary Flows in Jet-driven Vortex Tubes. J. Aerospace Sci. 29, 1142 (1962).

9. D. H. Ross, An Experimental Study of Secondary Flow in Jet-driven Vortex Chambers. Report No. ATN-64 (9227)-1 (1964).

10. O. L. Anderson, Theoretical Solutions for the Secondary Flow on the End Wall of a Vortex Tube. Report R-2494-1, United Aircraft Corporation Research Laboratories (1961).

11. O. L. Anderson, Theoretical Effect of Mach Number and Temperature Gradient on Primary and Secondary Flows in a Jet-driven Vortex. Report RTD-TDR-63-1098, United Aircraft Corporation Research Laboratories (1963).

12. W. S. Lewellen, Three-Dimensional Viscous Vortices in Incompressible Flow. Thesis, 64-8331 (University Microfilms, Inc., Ann Arbor, Michigan, 1964).

Table 1

Parameters used for calculated curves

Fig.	No.	10^2 x L moles/sec			n	b	m	z_h/z_c	$\frac{L_{wc}}{L}$	$\frac{L_{wh}}{L}$	$N_{wc}-N_o$ x 10^5	$N_{wh}-N_o$ x 10^5
		$\theta=0$	$\theta=\theta_o$	$\theta=1$								
11	I	2.7	2.7	2.7	-0.5	0.3	3.3	1	0.03	0.1	-13	- 8
	II	2.7	2.7	2.6	-0.5	0.3	2.5	1	0.03	0.1	-13	- 7
	III	2.0	2.7	2.7	-0.5	0.35	3.0	1	0.01	0.1	- 4	- 4
12	I	1.4	2.3	2.1	-0.5	0.3	3.0	11	0.03	0.1	- 5	- 6
	II	2.7	2.7	2.7	-0.5	0.3	3.0	1	0.03	0.2	- 4	-12
13	I	2.4	2.5	2.2	-1.0	0.2	3.0	0.05	0.01	0.1	- 5	- 6
	II	2.7	2.7	2.7	-0.3	0.3	4.0	0.2	0.01	0.1	- 4	- 7
	III	2.7	2.7	2.7	0	0.3	3.0	1	0.05	0.1	- 4	- 7

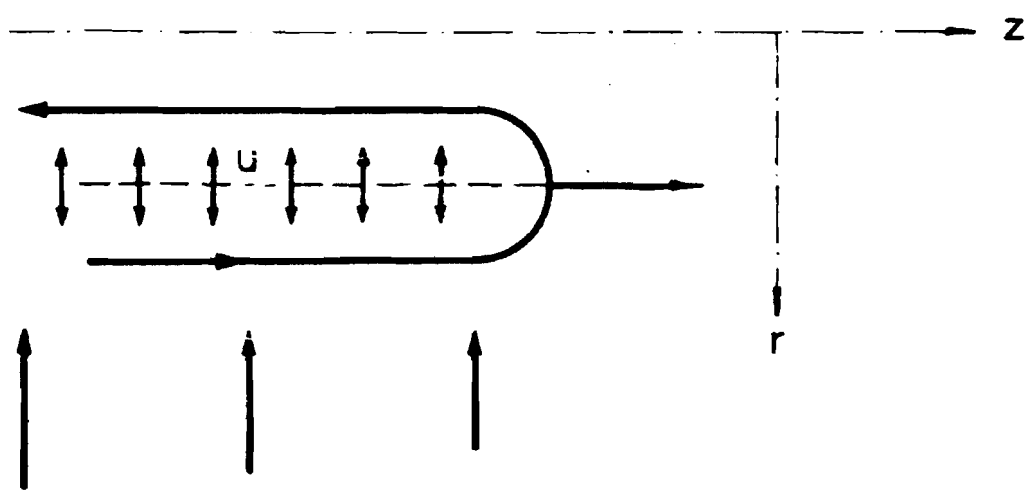

Fig. 1. Counter-current exchange.

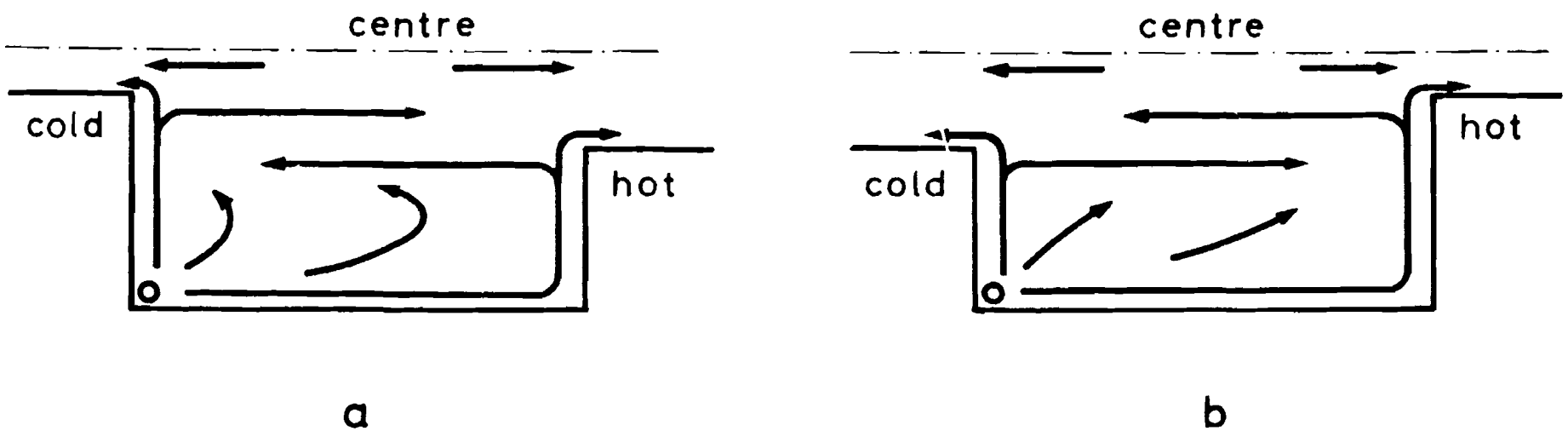

Fig. 2. Basic secondary-flow patterns.

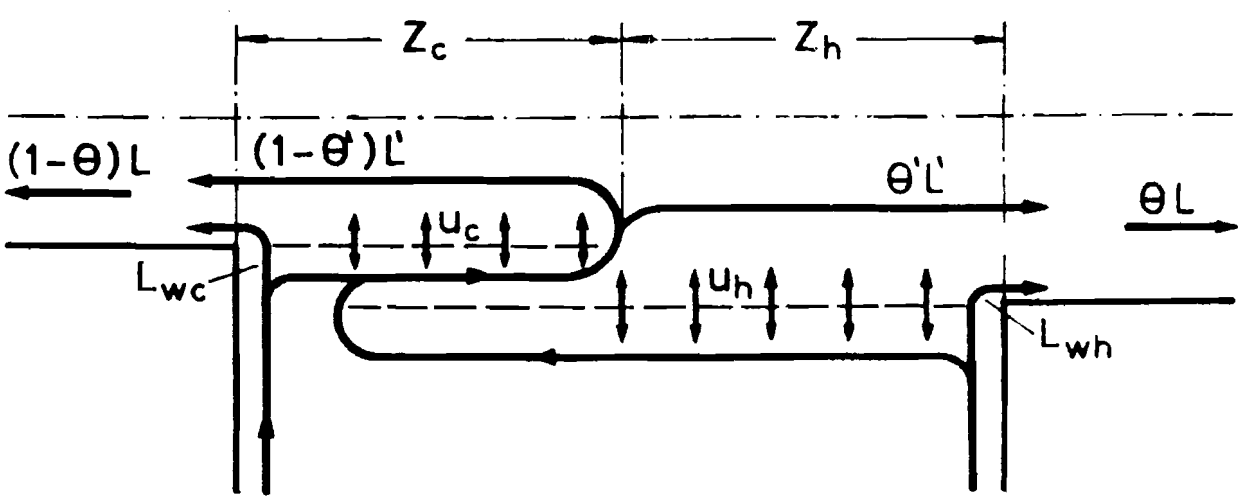

Fig. 3. Schematic representation of separation exchange regions when both valves are open ($\theta = \theta_o$).

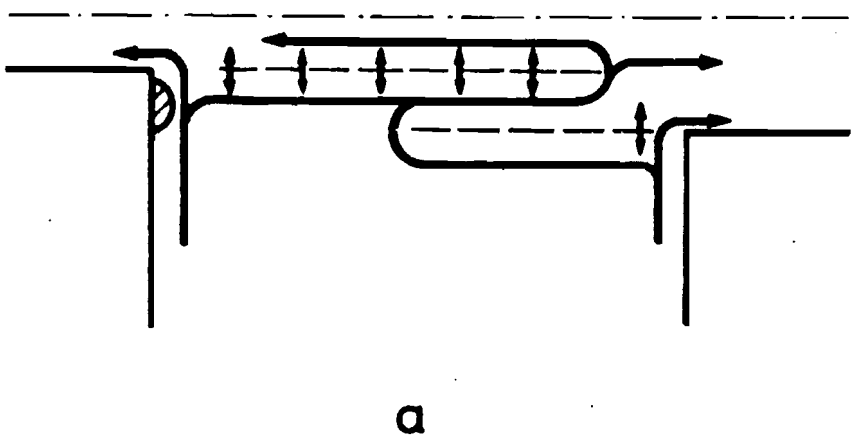

a

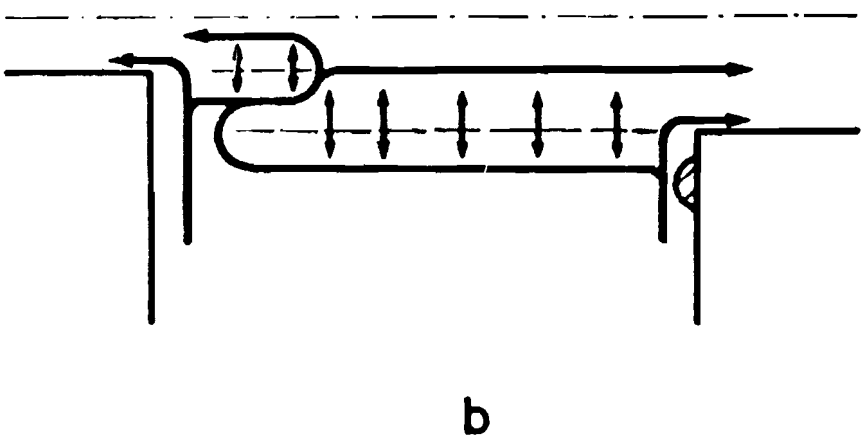

b

Fig. 4. Effect of end-wall surface conditions on secondary flows and separative exchange.

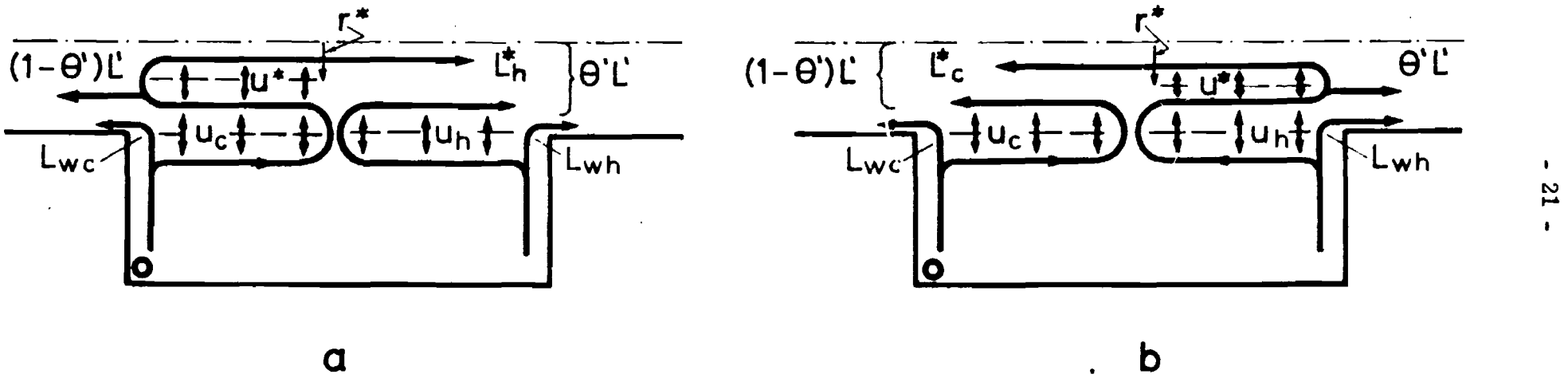

Fig. 5. Schematic representation of separative exchange when (a) $\theta > \theta_o$, and (b) $\theta < \theta_o$.

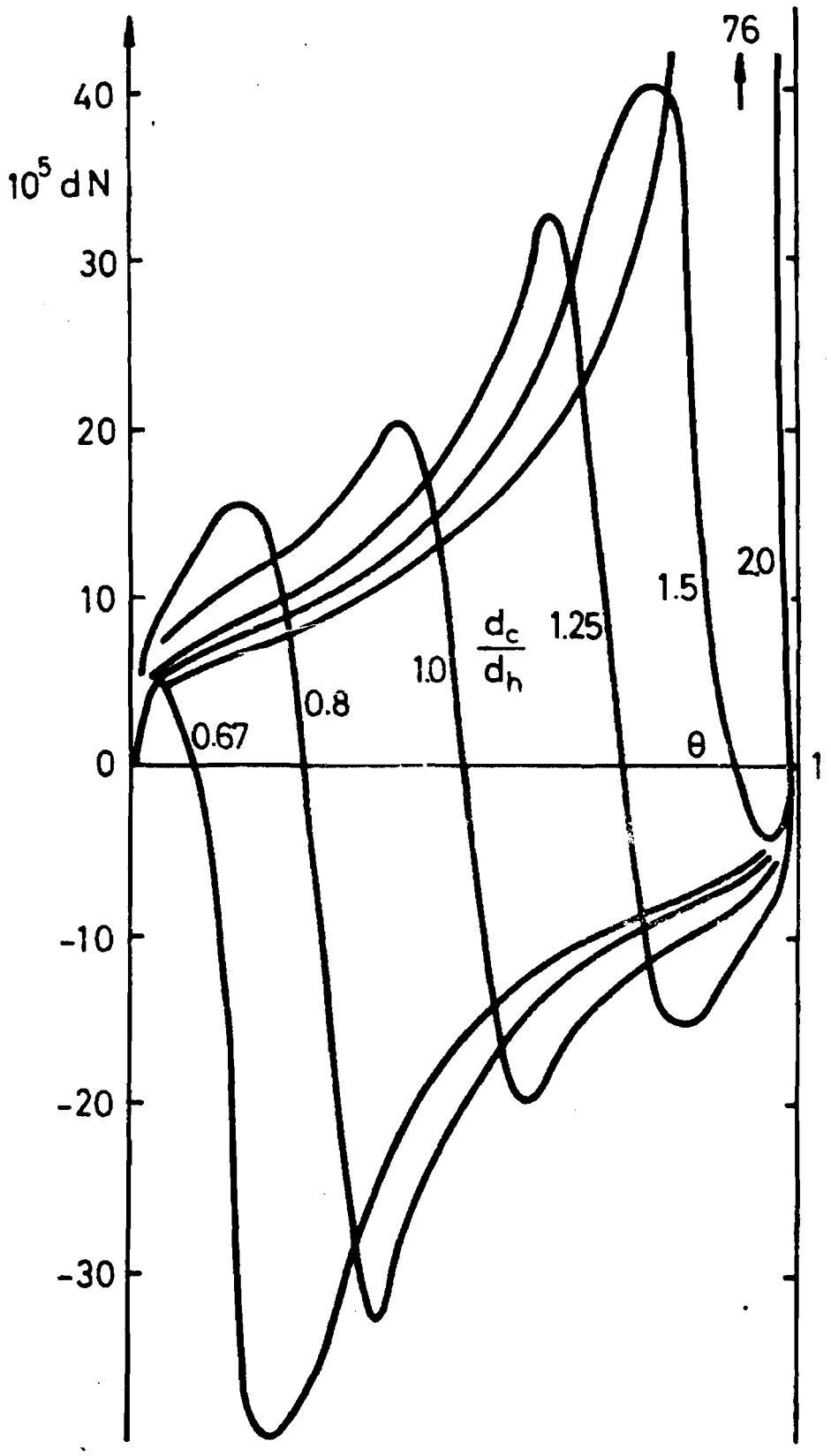

Fig. 6. Calculated gas separation. Effect of changing d_h/d_c. D = 10 mm; z_o = 6 cm; $d_c + d_h$ between 3 and 4 mm; L, v_j, b(= 0.25), n(= - 0.5) as in experiments; m = 4; $L_{wc} = L_{wh}$ = 0.01 L; $N_{wc} - N_o = N_{wh} - N_o = 0$; $z_h/z_c = 1$.

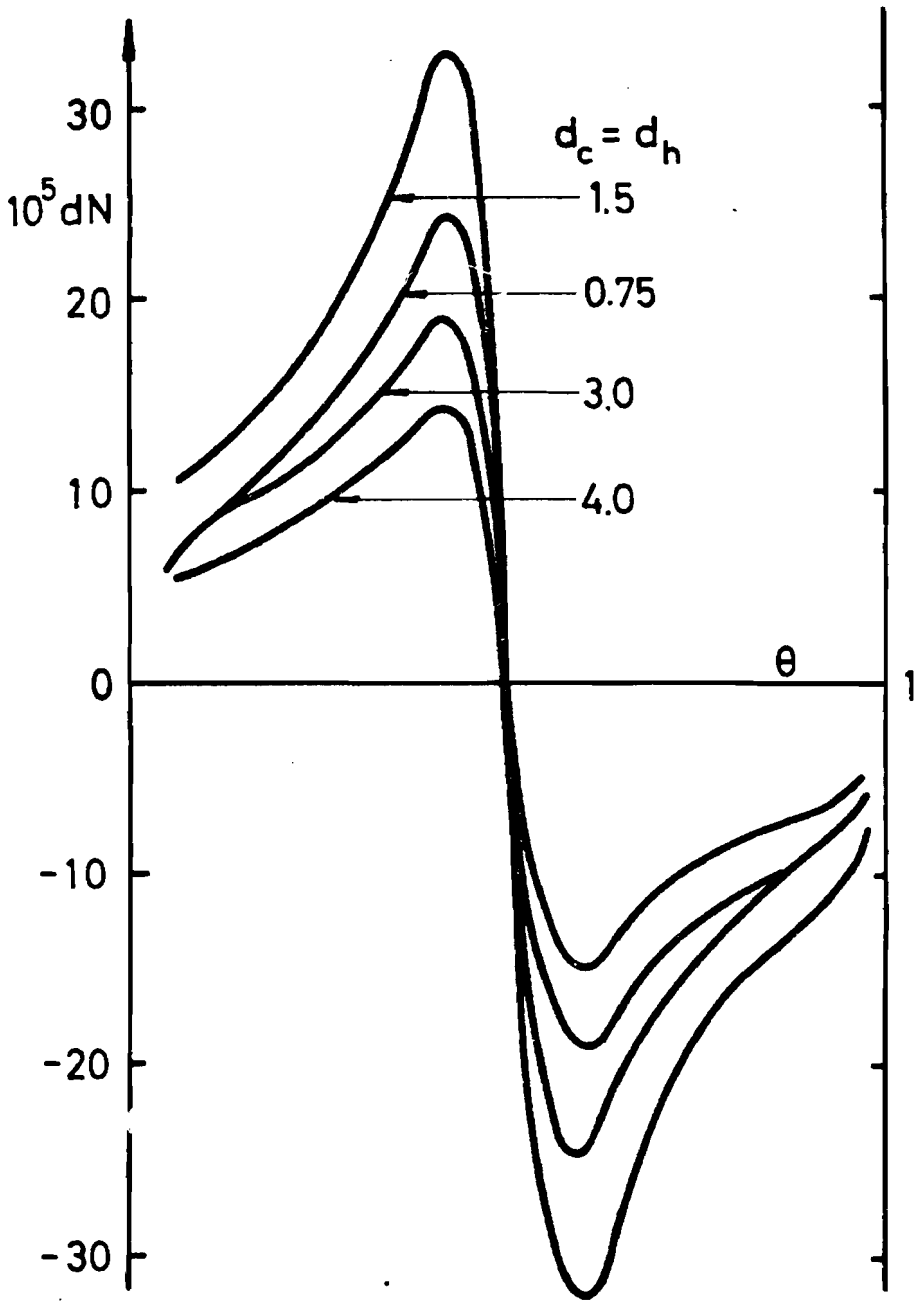

Fig. 7. Calculated gas separation. Effect of changing $d_c + d_h$.
D = 10 mm; z_o = 6 cm; $d_c = d_h$; b = 0.3; otherwise as in fig. 6.

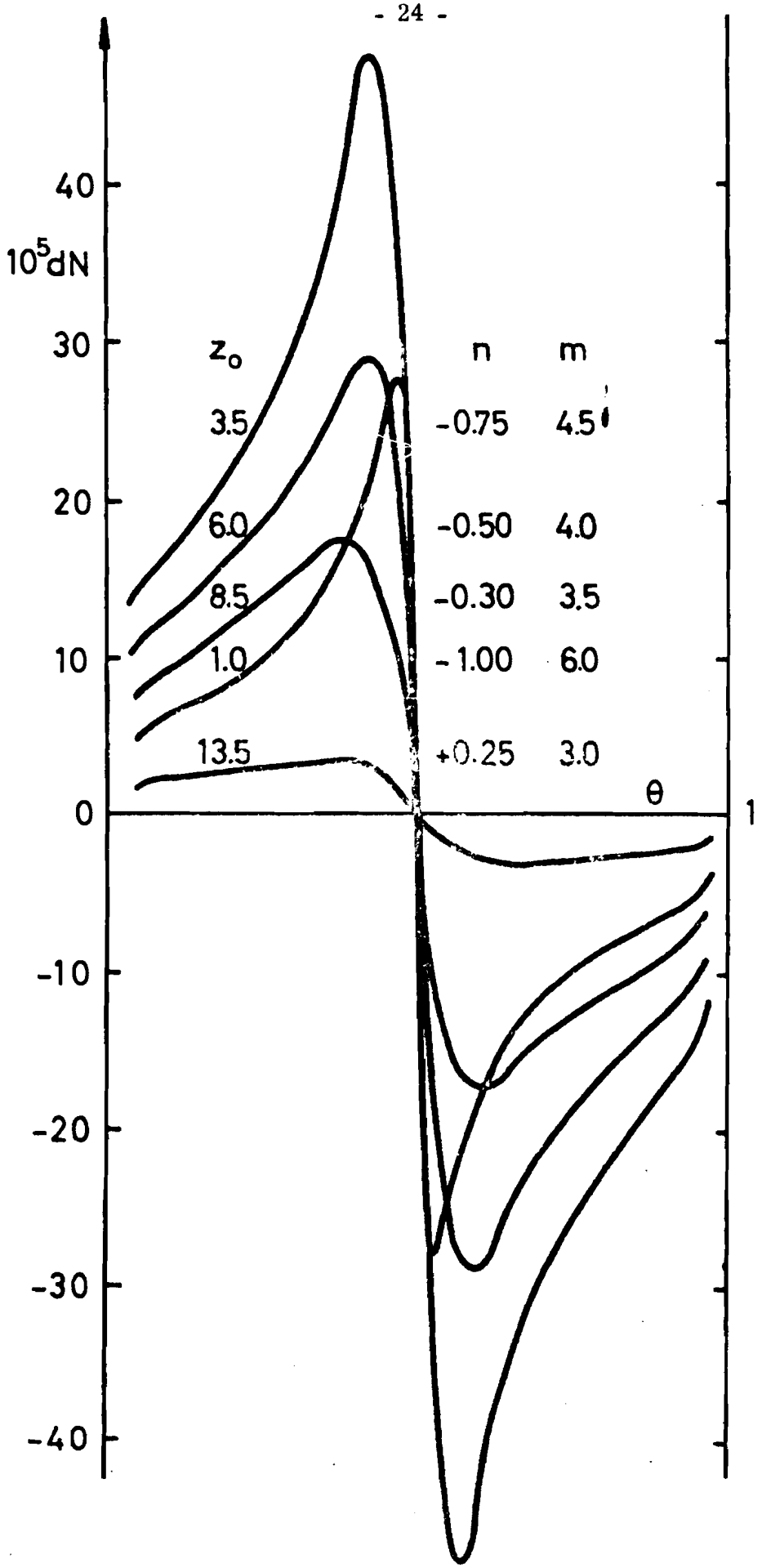

Fig. 8. Calculated gas separation. Effect of changing z_o. D = 10 mm; $d_c = d_h$ = 2 mm; b = 0.3; L and v_j as in experiments; m and n as indicated (estimated values); $L_{wc} = L_{wh}$ = 0.01 L; $N_{wc} - N_o = N_{wh} - N_o = 0$; $z_h/z_c = 1$.

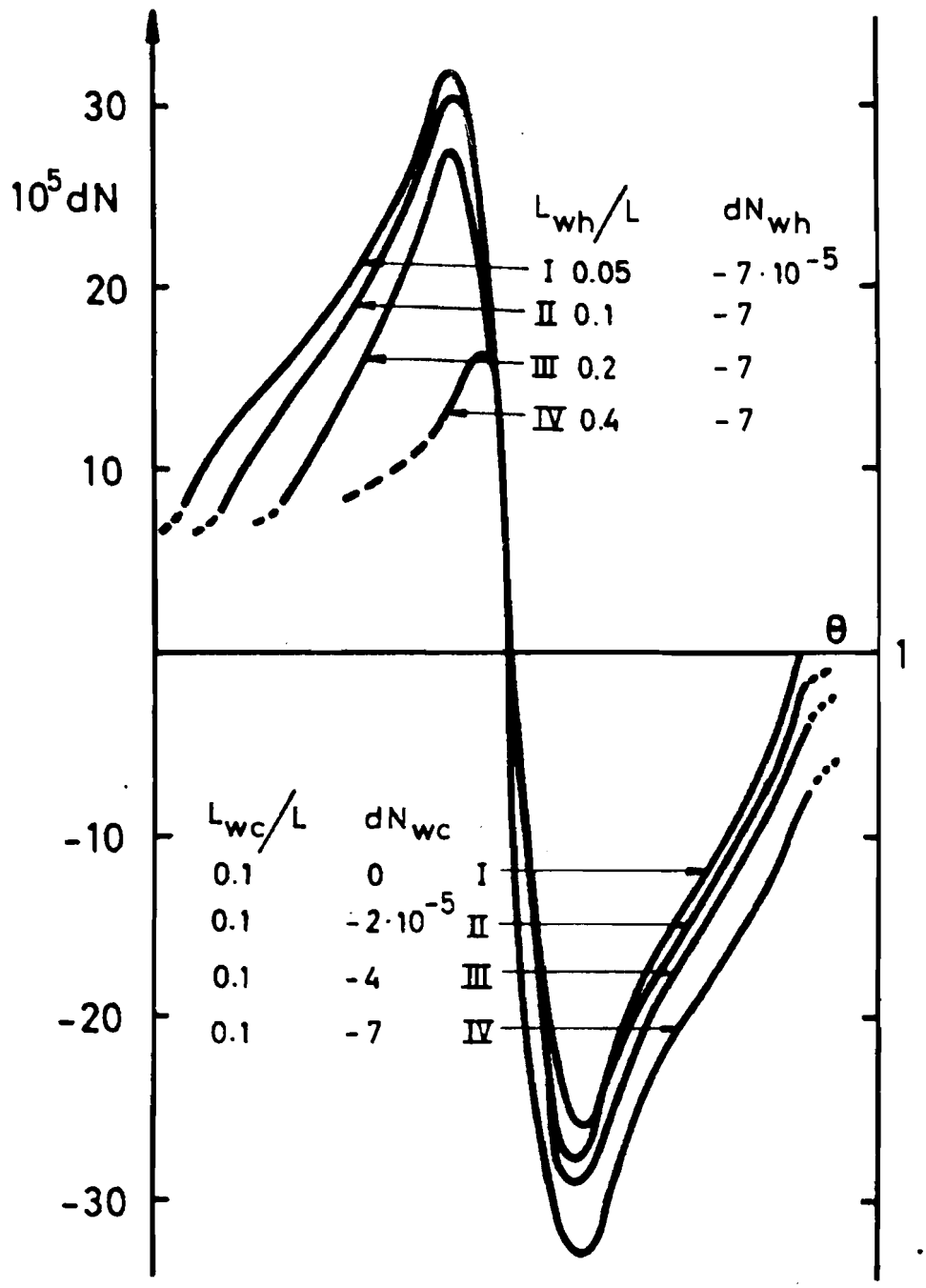

Fig. 9. Calculated gas separation. D = 10 mm; z_o = 6 cm; $d_c = d_h$ = 2 mm; b = 0.3; L and v_j as in experiments; n = - 0.5; m = 4; z_h/z_c = 1; $dN_{wc} = N_{wc} - N_o$; $dN_{wh} = N_{wh} - N_o$.

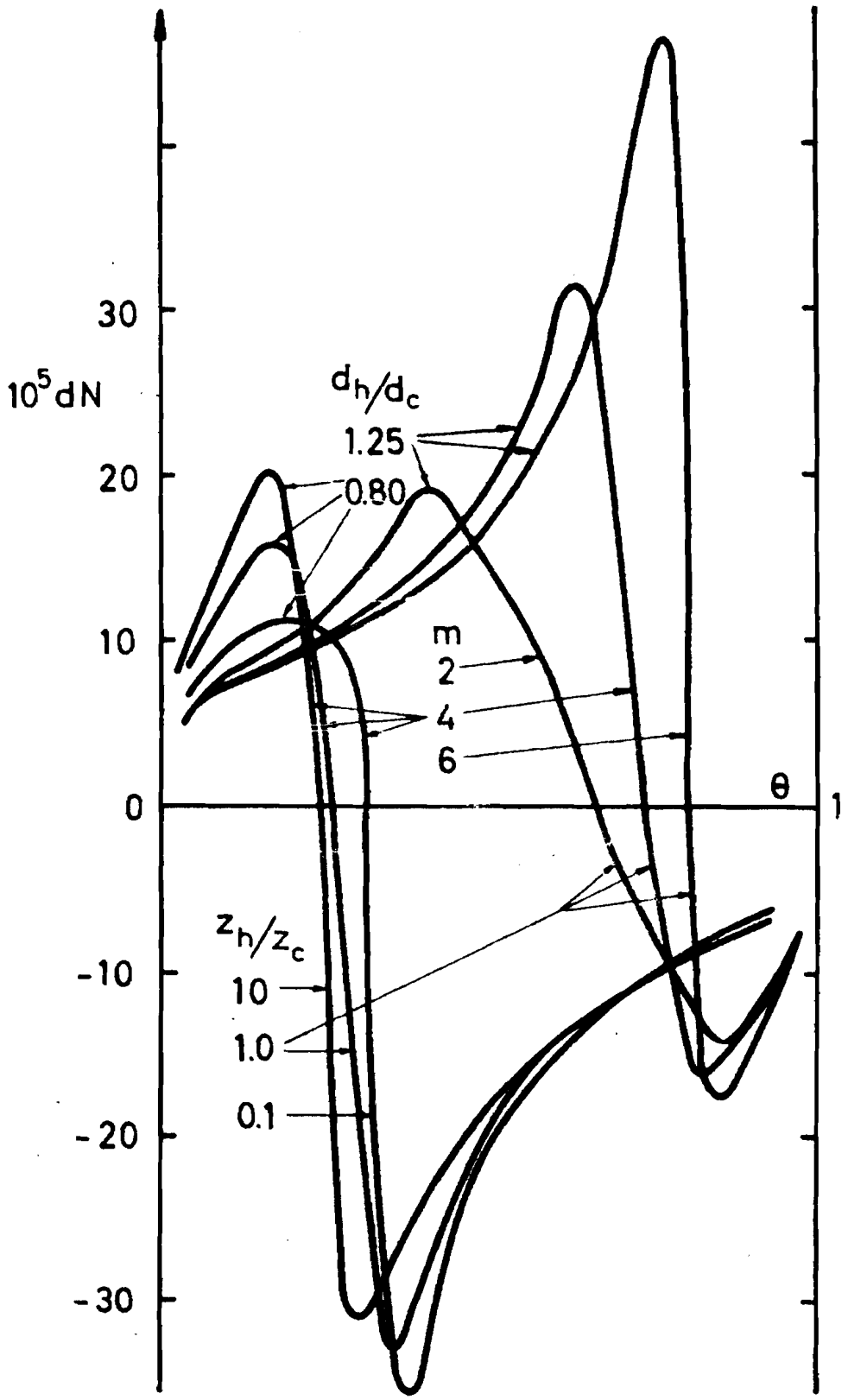

Fig. 10. Calculated gas separation. D = 10 mm; z_o = 6 cm; $d_c + d_h$ = 3.4 mm; b = 0.25; L and v_j as in experiments; n = - 0.5; $L_{wc} = L_{wh} = 0.01$ L; $N_{wc} - N_o = N_{wh} - N_o = 0$.

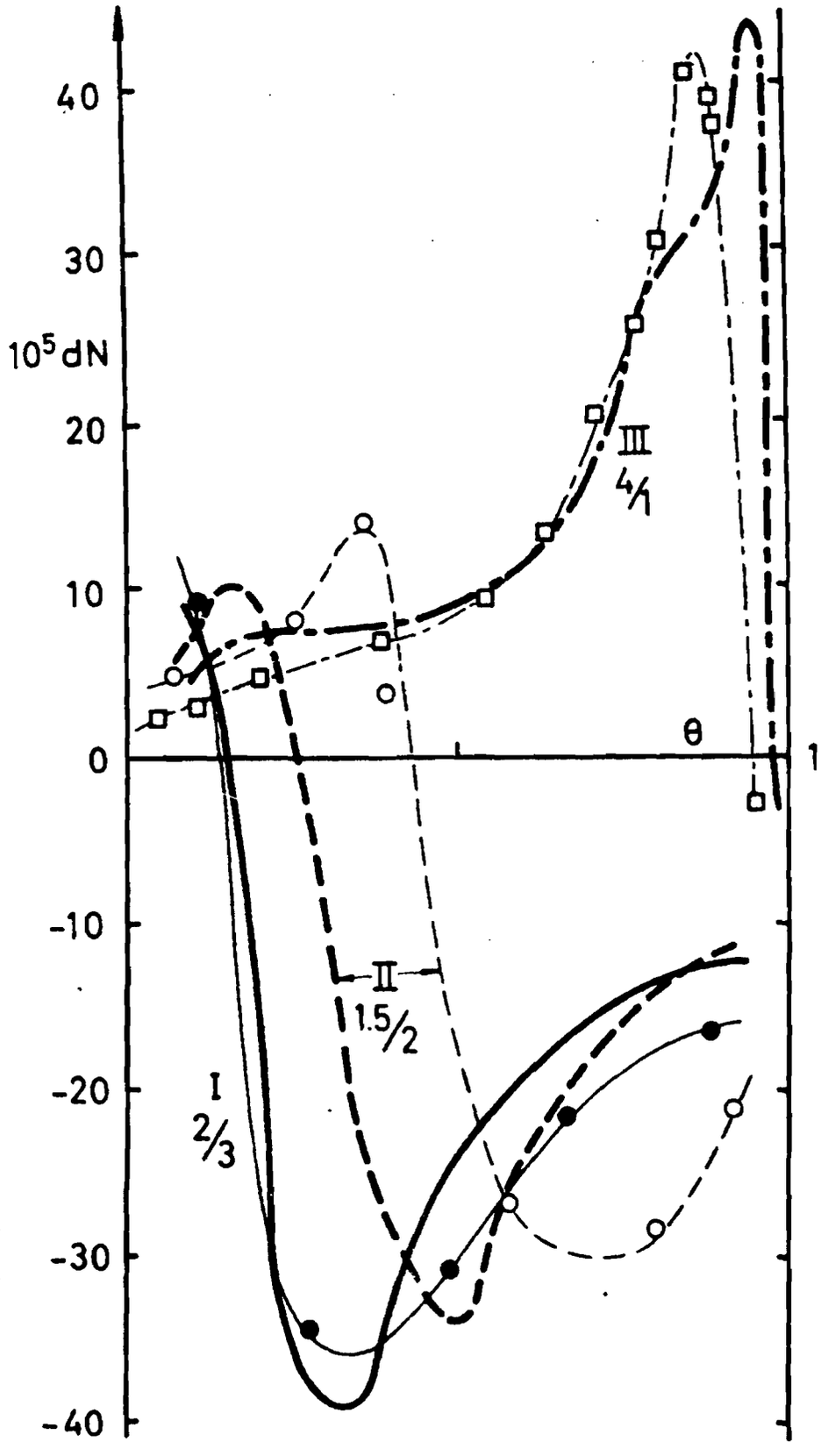

Fig. 11. Comparison between calculated and experimental gas separation, cf. fig. 6. D = 10 mm; z_o = 6 cm; ratios indicate d_h(mm)/d_c(mm); L and v_j from the experiment; thin lines connect experimental points; see table 1 for further details.

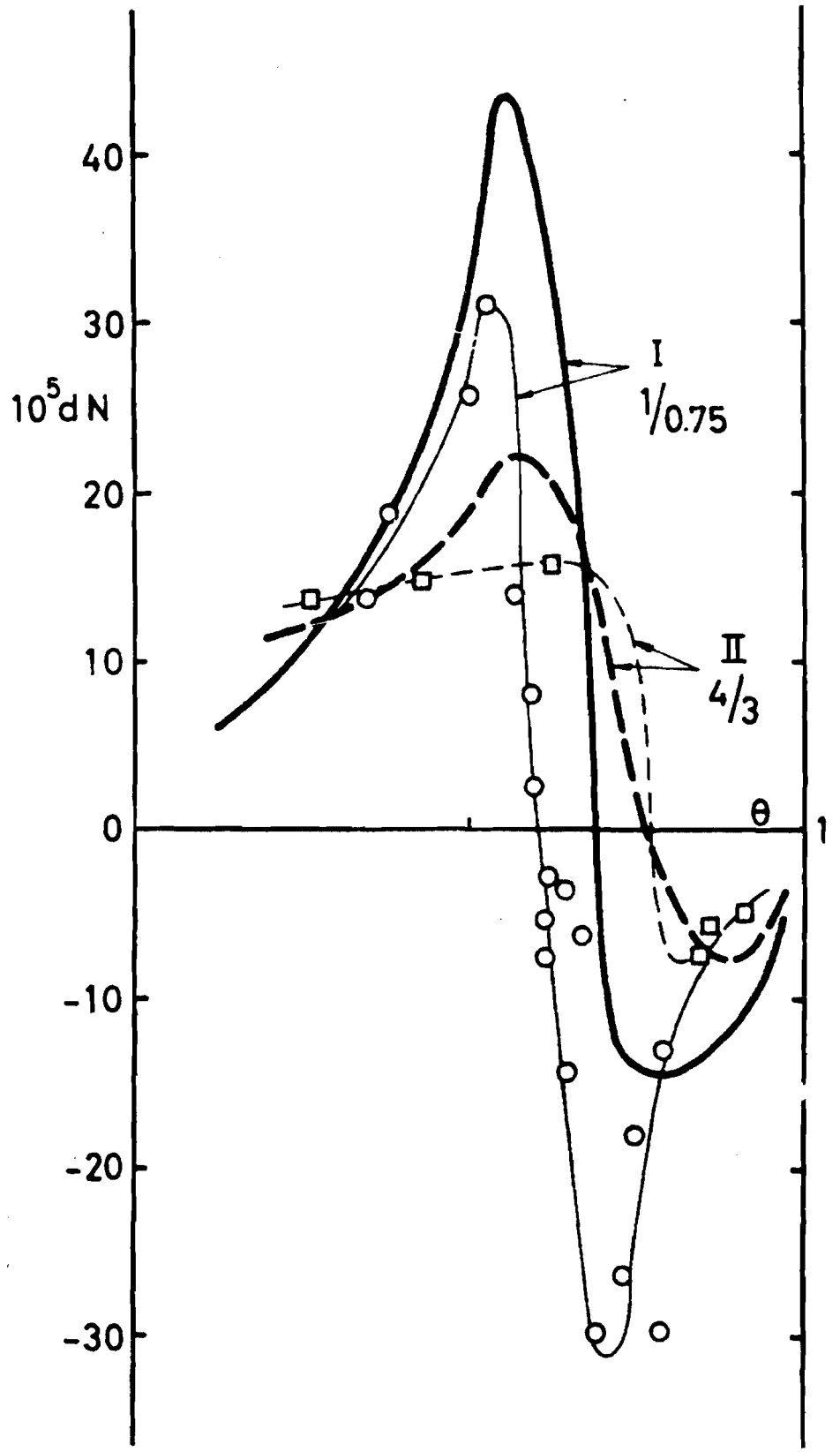

Fig. 12. Comparison between calculated and experimental gas separation, cf. fig. 7. $d_h/d_c = 1.33$; see caption to fig. 11.

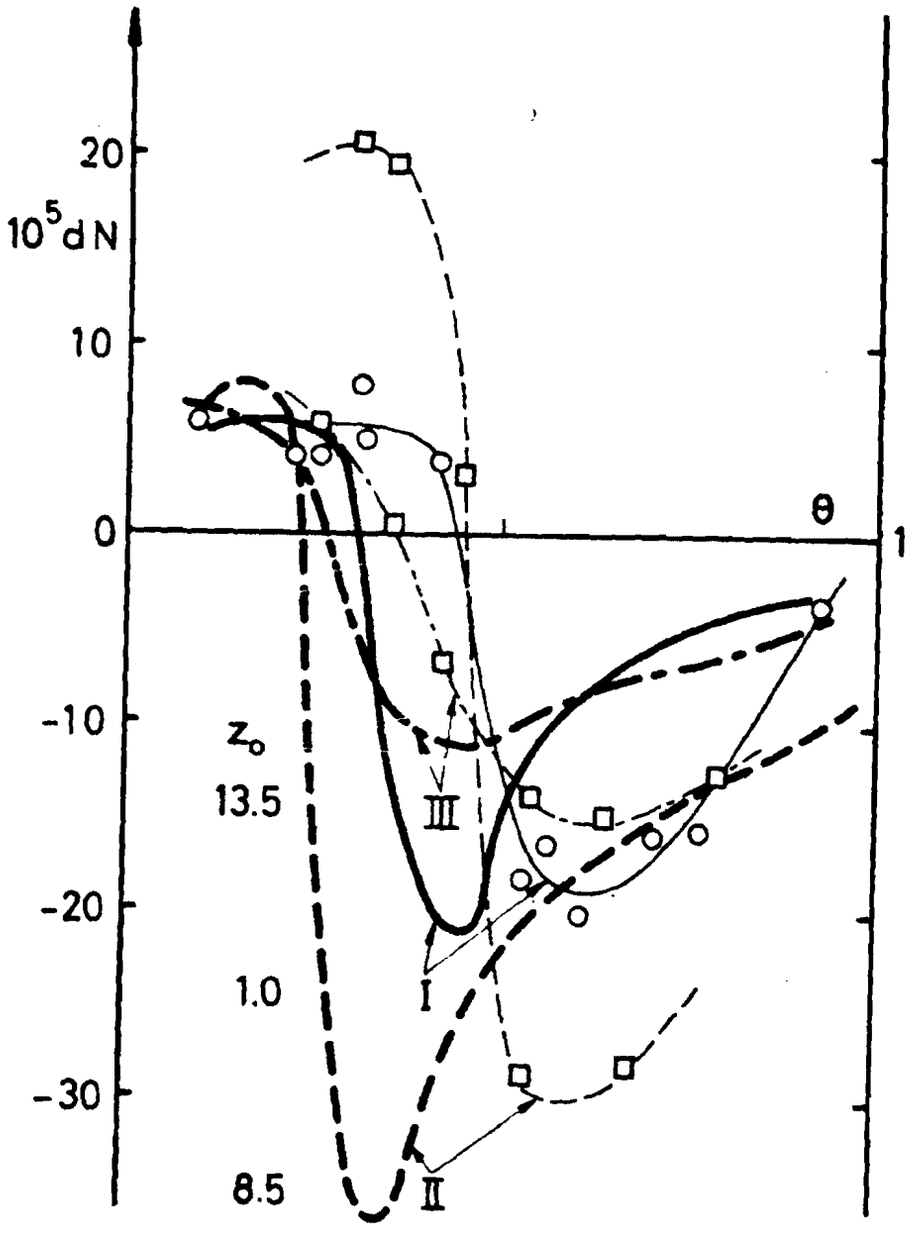

Fig. 13. Comparison between calculated and experimental gas separation, cf. fig. 8. D = 10 mm; d_c = 2 mm; d_h = 1.5 mm; z_o (in cm) as indicated; see also curve II, fig. 11; L and v_j from the experiment; thin lines connect experimental points; see table 1 for further details.

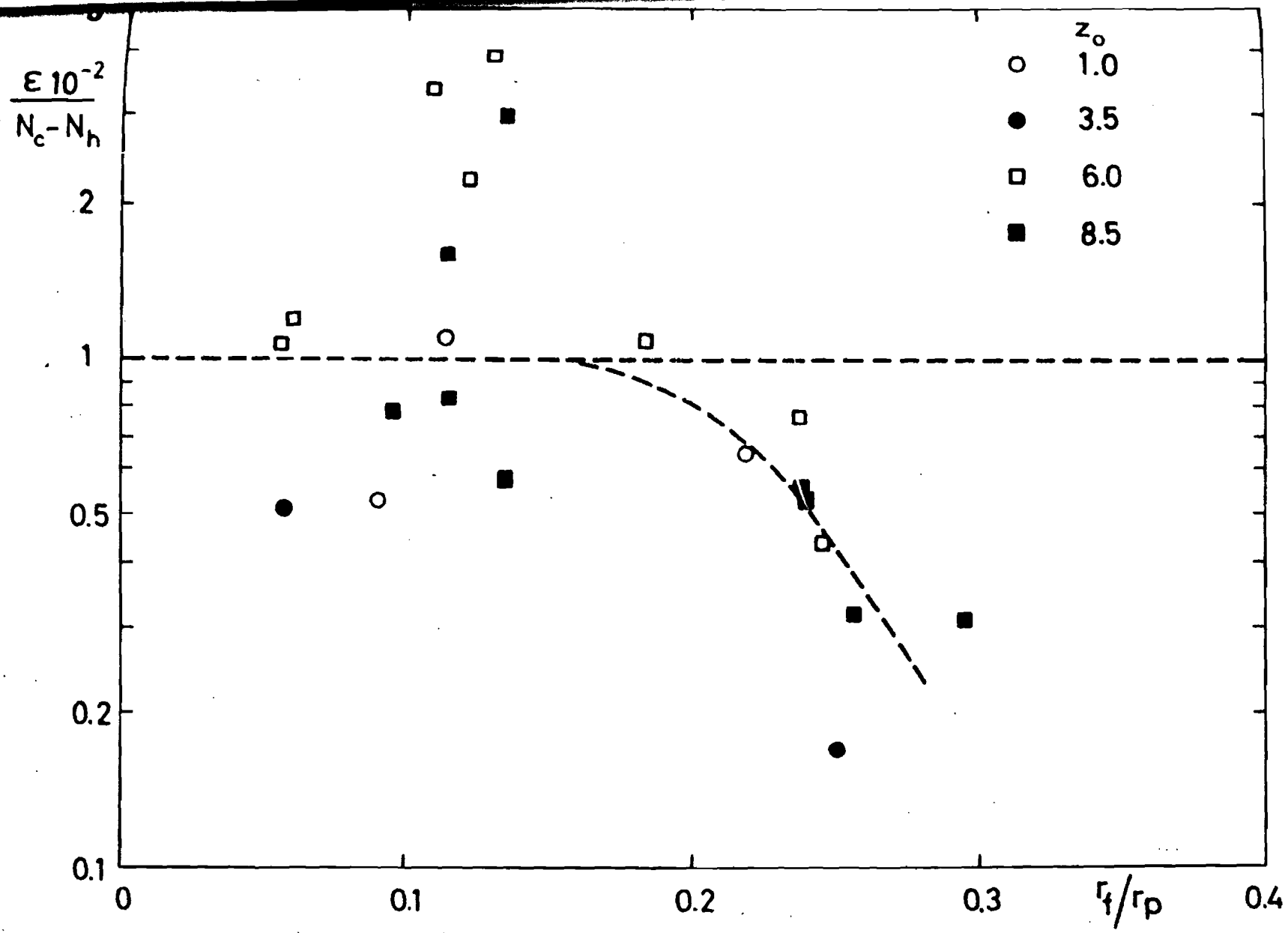

Fig. 14. Ratios of experimental to calculated gas separation effects. ε is the measured difference in oxygen content between the outgoing streams in per cent (v/v) absolute.